THE JOURNAL OF BIOLOGICAL CHEMISTRY VOL. 289, NO. 23, pp. 16148–16163, June 6, 2014

Rabies Virus Envelope Glycoprotein Targets Lentiviral Vectors to the Axonal Retrograde Pathway in Motor Neurons*[S]

Received for publication, January 13, 2014, and in revised form, April 11, 2014 Published, JBC Papers in Press, April 21, 2014, DOI 10.1074/jbc.M114.549980

James N. Hislop[‡1,2], Tarin A. Islam[‡1], Ioanna Eleftheriadou[‡], David C. J. Carpentier[‡3], Antonio Trabalza[‡], Michael Parkinson[§], Giampietro Schiavo[§¶], and Nicholas D. Mazarakis[‡4]

From [‡]Gene Therapy, Centre for Neuroinflammation and Neurodegeneration, Division of Brain Sciences, Department of Medicine, Imperial College London, Du Cane Road, London W12 0NN, United Kingdom, [§]Molecular NeuroPathoBiology Laboratory, Cancer Research UK London Research Institute, Lincoln's Inn Fields Laboratories, 44 Lincoln's Inn Fields, London WC2A 3LY, United Kingdom, and [¶]Sobell Department of Motor Neuroscience and Movement Disorders, UCL Institute of Neurology, University College London, Queen Square, London WC1N 3BG, United Kingdom

Background: Trafficking pathways underlying retrograde transduction of neurons with lentiviral vectors carrying the rabies G glycoprotein are uncharted, and barriers to high transduction efficiencies are undefined.
Results: Vectors are internalized through cognate receptors and transported to the soma by fast axonal transport in pH-neutral endosomes.
Conclusion: The major barrier to axonal transduction is postaxonal transport.
Significance: Enhancing endosomal escape will be a novel area for improvement of gene therapy vector transduction efficiency.

Rabies pseudotyped lentiviral vectors have great potential in gene therapy, not least because of their ability to transduce neurons following their distal axonal application. However, very little is known about the molecular processes that underlie their retrograde transport and cell transduction. Using multiple labeling techniques and confocal microscopy, we demonstrated that pseudotyping with rabies virus envelope glycoprotein (RV-G) enabled the axonal retrograde transport of two distinct subtypes of lentiviral vector in motor neuron cultures. Analysis of this process revealed that these vectors trafficked through Rab5-positive endosomes and accumulated within a non-acidic Rab7 compartment. RV-G pseudotyped vectors were co-transported with both the tetanus neurotoxin-binding fragment and the membrane proteins thought to mediate rabies virus endocytosis (neural cell adhesion molecule, nicotinic acetylcholine receptor, and p75 neurotrophin receptor), thus demonstrating that pseudotyping with RV-G targets lentiviral vectors for transport along the same pathway exploited by several toxins and viruses. Using motor neurons cultured in compartmentalized chambers, we demonstrated that axonal retrograde transport of these vectors was rapid and efficient; however, it was not able to transduce the targeted neurons efficiently, suggesting that impairment in processes occurring after arrival of the viral vector in the soma is responsible for the low transduction efficiency seen *in vivo*, which suggests a novel area for improvement of gene therapy vectors.

Lentivirus-mediated delivery is a highly promising technique for gene therapy showing significant advantages over other viral delivery vectors by their ability to effectively transduce non-dividing cells such as neurons (1, 2). An additional advantage is represented by the possibility to utilize heterologous envelope glycoproteins to pseudotype these vectors, thus broadening their tropism (3). Among the first and most widely used envelope glycoproteins for pseudotyping lentiviral vectors is the vesicular stomatitis virus glycoprotein (VSV-G).[5] Because of their high transduction efficiency, wide cell tropism, and stability, VSV-G pseudotyped lentivirus vectors are considered the gold standard for the field. Their broad tropism, however, diminishes their usefulness for gene targeting to specific disease sites. In addition, they lack the ability to access the central nervous system (CNS) without invasive delivery methods.

Pseudotyping lentiviral vectors with the rabies virus envelope glycoprotein (RV-G) makes them neurotropic and more importantly confers upon them the ability to retrogradely traffic along axons to neuronal soma (4). Furthermore, peripheral administration of RV-G lentiviral vectors to the rat gastrocnemius muscle leads to gene transfer in motor neurons of the lumbar spinal cord (4). The specific targeting of neuronal cells

* This work was supported by Seventh Framework Programme European Research Council Advanced Investigators Grant 23314 (to N. D. M. supporting J. N. H., T. A. I., I. E., A. T., and D. C. J. C.), Imperial College funds (to N. D. M.), and Cancer Research UK (to M. P., K. B., and G. S.).
[S] This article contains supplemental Figs. 1–9 and Movies 1–7.
[1] Both authors contributed equally to this work.
[2] Present address: School of Medical Sciences, College of Life Sciences and Medicine, University of Aberdeen, Inst. of Medical Sciences, Foresterhill, Aberdeen AB25 2ZD, Scotland, UK.
[3] Present address: Dept. of Pathology, University of Cambridge, Tennis Court Rd., Cambridge CB2 1QP, UK.
[4] To whom correspondence should be addressed. E-mail: n.mazarakis@imperial.ac.uk.

[5] The abbreviations used are: VSV-G, vesicular stomatitis virus glycoprotein; RV-G, rabies virus envelope glycoprotein; $p75^{NTR}$, p75 neurotrophin receptor; NCAM, neural cell adhesion molecule; nAChR, nicotinic acetylcholine receptor; HIV-1, human immunodeficiency virus, type 1; TeNT, tetanus neurotoxin; EIAV, equine infectious anemia virus; eGFP, enhanced green fluorescent protein; FlAsH, fluorescein arsenical hairpin binder; PFA, paraformaldehyde; m.o.i., multiplicity of infection; IN, integrase; MFC, microfluidic chamber; DIV, days *in vitro*; Hc, binding fragment of TeNT.

with the RV-G pseudotype opens up the possibility of non-invasive, distal administration of the vector at the neuromuscular synapses to target cells of the CNS affected by motor neuron diseases such as amyotrophic lateral sclerosis and spinal muscular atrophy. In this respect, lentiviral delivery of transgenes or RNAi using such vectors has been shown to be effective in ameliorating symptoms in murine models of amyotrophic lateral sclerosis and spinal muscular atrophy (5, 6). Despite the clear advantages of this system for gene therapy, a number of improvements are still required before pursuing clinical trials. One established strategy for improving the efficiency of transduction is the manipulation of the viral envelope, a process known as surface engineering (7). However, a more general approach is the identification of the molecular processes involved in retrograde viral transduction to identify the exact limitations of this therapeutic vehicle. Currently, no detailed study on lentiviral vector trafficking has been attempted.

Rhabdoviruses such as rabies virus and VSV enter cells using a well studied mechanism (8). Following binding to a cell surface molecule (p75 neurotrophin receptor ($p75^{NTR}$), neural cell adhesion molecule (NCAM), and nicotinic acetylcholine receptor (nAChR) for RV), virus particles undergo clathrin-mediated endocytosis. Following uptake, clathrin-coated vesicles become associated with the small GTPase Rab5, and their lumen undergoes acidification. "Endosomal maturation" promotes an increased association with Rab7 (rather than Rab5) and is accompanied by a further decrease in pH before the endosome finally fuses with the lysosome (9, 10). Importantly, the viral particles "escape" from the endosomal lumen before fusion with the lysosome, a process that is triggered by acidification (11, 12). This acidic environment induces a conformational change in the viral glycoprotein that initiates membrane fusion between the viral envelope and the endosomal membrane, allowing escape of the viral capsid. In wild-type rabies virus, the capsid then enters the cytosol, a process enhanced by an interaction of the capsid with the cytoplasmic dynein motor complex, which promotes transport toward the soma (13–15), a process that can occur even from distal axonal sites. In addition, transport of enveloped rabies virus in neuronal transport vesicles has been demonstrated *in vitro* (16). Previous experiments have studied the trafficking of labeled HIV-1 and demonstrated that HIV-1 capsids are also able to undergo dynein-mediated trafficking to the nucleus (17, 18); however, because native HIV-1 is unable to infect neurons (for a review, see Ref. 19), it is currently unclear whether these capsids can reach the nucleus from such distal sites as the neuromuscular junction.

Recent work has characterized an axon-specific membrane trafficking pathway (20, 21). This pathway is utilized by tetanus neurotoxin (TeNT) and enables this and other pathogens to reach the neuron soma from distal infection sites such as the neuromuscular junction (22–28). This axonal trafficking pathway, shared by neurotrophins in the CNS (29), utilizes a population of endosomes undergoing a sequential Rab5 and Rab7 transition. In contrast to the canonical pathway, however, this maturation is not accompanied by a decrease in the luminal pH, which remains neutral. Interestingly, it has been recently demonstrated that two of the reported receptors for RV-G ($p75^{NTR}$ and NCAM) undergo retrograde axonal transport in these Rab7-positive non-acidified endosomes (23, 30), thus suggesting a potential route of delivery for both wild-type rabies virus and RV-G pseudotyped lentiviral vectors that would allow the vector to reach the nucleus without pH-driven endosomal fusion.

Here, we investigated the endocytic trafficking of RV-G pseudotyped vectors in motor neurons. Utilizing a number of distinct labeling techniques, we showed that these vectors did indeed undergo axonal retrograde transport in primary motor neurons. We further demonstrated that this transport was achieved through sequential Rab5- and Rab7-positive organelles also used for the long range transport of $p75^{NTR}$, and the nAChR was also targeted to the same retrograde trafficking pathway. We further managed to recapitulate retrograde transport in primary motor neurons cultured in microfluidic chambers but failed to detect robust transduction under similar conditions. Use of this *in vitro* system, which parallels the *in vivo* intramuscular injection route, strongly suggests that the major block to efficient viral vector transduction is at a stage following axonal transport perhaps between endosomal escape and nuclear transport of the vector capsid.

EXPERIMENTAL PROCEDURES

Cell Lines and Culture—HEK293T cells were from ATCC UK and cultured in DMEM supplemented with 10% FBS, 1% penicillin/streptomycin (Sigma), and 1% L-glutamine (Sigma). The NSC-34 mouse neuroblastoma cell line was a gift from Pam Shaw (University of Sheffield, UK) and was maintained in DMEM supplemented with 10% FBS, 1% essential amino acids (Sigma), and 1% penicillin/streptomycin and routinely passaged every 72–96 h. NSC-34 cells were differentiated by culturing in low serum DMEM (1% FBS, 1% essential amino acids, and 1% penicillin/streptomycin) for 96 h. Antibodies used were NCAM (Millipore; 1:1,000), nAChR (Abcam; 1:1,000), $p75^{NTR}$ (Cancer Research UK; 1:1,500), Rab5 (Abcam; 1:1,000), Rab7 (Cancer Research UK; 1:1,000), HIV-1 p24 (Abcam; 1:1,000), EIAV p26 serum (1:1,000; a kind gift from R. C. Montelaro, University of Pittsburgh School of Medicine), rabies virus glycoprotein (Abcam; 1:1,000), enhanced green fluorescent protein (eGFP) (1:1,000; Abcam, ab290), SMI32 (1:1,000; Covance, E11 CF00693), and VSV glycoprotein (1:250; Chongqing Biospes, BTL1023). Alexa Fluor® 647-conjugated α-bungarotoxin (1:500) and LysoTracker DND (1:100,000) were from Invitrogen, and Alexa Fluor 647-labeled anti-$p75^{NTR}$ and Alexa Fluor 555-labeled TeNT H_c have been described previously (23).

Cloning of Tagged Vector Plasmids—To produce a C-terminal fusion of the integrase gene product of the HIV-1 *pol* gene, PCR was used to remove the stop codon at the 3′-end of the *pol* gene in pMD2-LgpRRE and insert an XbaI site. The resulting product was digested with AflII and BspEI and used to replace the corresponding sequence in the pMD2-LgpRRE vector. PCR was then used to amplify the coding sequence of the eGFP of pEGFP-N1 (Clontech), and this sequence was then ligated in-frame between the new XbaI and BspEI sites.

Tetracysteine (Cys_4)-tagged *gag* constructs were made by splicing by overhang extension (31, 32) utilizing the plasmids pMD2-LgpRRE (for HIV-1 Cys_4) and pEV53B (for EIAV Cys_4). These were used as both the template for PCR cloning and the

final destination vector for the construct. The region containing the ClaI-BclI fragment of pMD-LgpRRE and SacII/AscI-XbaI fragment of pEV53B was amplified by PCR to generate *gag*-Cys_4 fragments that were cloned into pCRII (Invitrogen) by TOPO cloning. Following restriction enzyme digests and sequence analysis to identify clones with correct inserts, the *gag*-Cys_4 fragments were subcloned into their respective pMD2-LgpRRE and pEV53B vectors.

Production and Purification of Lentiviral Vectors—HIV-based lentiviral vectors were produced using a four-vector system as described previously (33). Briefly, HEK293T cells were plated in 3 × 150-mm dishes at a density of 1.4×10^6 cells/plate. 24 h later each plate was transfected with 15 μg of pLV-LacZ (Addgene) or *Sin-cPPT-PGK-eGFP-WHV* obtained from Professor Mimoun Azzouz (University of Sheffield, UK), 15 μg of HIV-1 GagPol (pMD2-LgpRRE, pMD2-Lgp(4C-MAC)RRE, or pMD2-LgpRRE-IN-GFP), 3 μg of HIV-1 Rev (pRSV-Rev obtained from Professor James Uney, University of Bristol, UK), and 5.1 μg of the envelope plasmid (pMD2-VSVg or pMD2-B2C) using calcium phosphate precipitation. 16 h post-transfection the medium was replaced with DMEM supplemented with 2% FBS, 1% penicillin/streptomycin, 1% L-glutamine, and 10 mM sodium butyrate. Medium was harvested 36 h later, and virus was concentrated by ultracentrifugation at 87,000 × *g* for 2 h at 4 °C through a 20% sucrose cushion (34). The viral pellet was then resuspended in 50 μl of TSSM buffer (20 mM tromethamine, 100 mM NaCl, 10 mg ml^{-1} sucrose, 10 mg ml^{-1} mannitol). To label the particles with lipophilic dye (Vybrant DiO or DiD, Invitrogen), an additional step was added. 16 h post-transfection medium was replaced with Opti-MEM (Invitrogen) containing 3.7 μM Vybrant dye and incubated at 37 °C for 2 h before replacing with medium containing sodium butyrate as above. For FlAsH labeling, at the time of sodium butyrate induction, 1 μM FlAsH-EDT_2 (Invitrogen) was added to the low serum medium premixed with 12.5 μM 1,2-ethanedithiol (EDT; Sigma-Aldrich), and virus production was continued for a further 36 h. Free biarsenical dye, not incorporated into vectors, was removed by centrifugation through a sucrose cushion as described above.

For the Cys_4-tagged EIAV vectors, each plate was transfected with 22.5 μg of EIAV GagPol (pEV53B or pEV53B Cys_4-MA-C), 22.5 μg of SIN6.1CZW-LacZ or 6.1CeGFPW, and 13.5 μg of pMD2-B2C. Biological activity of lentiviral vector preps carrying eGFP was determined as described previously (34). For vector expressing the *LacZ* gene, HEK293T cells were plated in a 12-well plate at 300,000 cells/well. 24 h later cells were transduced with vector (plus 8 μg/ml Polybrene). 48 h post-transduction cells were washed and fixed in paraformaldehyde (PFA), and LacZ expression was detected using the β-Gal Staining kit (Invitrogen, K1465-01). Positive cells were then manually counted to determine the number of LacZ-forming units (LfU)/ml.

Preparation of Rat Primary Neuronal Cultures—Primary motor neurons were obtained and cultured as described previously (33). Briefly, all cells were plated onto culture vessels treated with 5 μg/ml poly-L-ornithine and 3 μg/ml laminin. Cells were plated in 8-well chamber slides and for live imaging were plated in glass-bottomed dishes (Mattek). Ventral spinal cords were removed from E14 embryos and placed in Hanks' balanced salt solution supplemented with 0.025% trypsin (Sigma) for 10 min at 37 °C. After digestion, 100 μl of DNase (Invitrogen; 1 mg/ml in L-15 medium), 100 μl of BSA fraction V (Sigma-Aldrich; 4% in L-15 medium), and 800 μl of L-15 medium were added to the tube, and clumps were mechanically dissociated. Cells were then centrifuged through a BSA cushion followed by further purification based on the relative large size of motor neurons and subsequent flotation on an Optiprep gradient.

All animal procedures were approved by the local Ethics Committee and performed in accordance with the United Kingdom Animals Scientific Procedures Act (1986) and associated guidelines. All efforts were made to minimize the number of animals used and the suffering. The animals were housed under a 12-h light/dark cycle (light phase, 7:00 p.m. to 7:00 a.m.) with food and water available *ad libitum*. Animals were supplied by Charles River, UK. Timed pregnant female Wistar rats on the 14th day of pregnancy (E14) were used in the experiment. Animals were sacrificed by intraperitoneal injection of 200 mg/kg sodium pentobarbitone, and the embryos were immediately removed and kept in modified Hanks' balanced salt solution (Ca^{2+}- and Mg^{2+}-free; Sigma-Aldrich).

In Vivo Intramuscular Injections of Lentiviral Vector—Small incisions in the right hind limb were performed to expose the gastrocnemius muscle. Concentrated RV-G pseudotyped lentiviral (10 μl of 1.66×10^9 transducing units/ml) eGFP-expressing vector and Fast Blue (3 μl of 2% solution in water) were intramuscularly injected unilaterally in right gastrocnemius muscle of C57BL/6 mice ($n = 6$) via two injections (lentiviral vector) or a single injection (Fast Blue) with a 26-gauge hypodermic needle connected to a microinjection pump (UltraMicroPump III and Micro4 Controller, World Precision Instruments) at a rate of 1 μg/μl. Three weeks or 8 days postinjection of lentiviral vector or Fast Blue, respectively, mice were sacrificed by intraperitoneal injection of 200 mg/kg sodium pentobarbitone and transcardially perfused with 10 ml of saline (0.9% (w/v) NaCl) plus heparin followed by 100 ml of 4% (w/v) PFA (Sigma-Aldrich) in PBS. Spinal cords were removed and post-fixed for 4 h in 4% PFA followed by cryoprotection in 10% glycerol and 20% sucrose in PBS for at least 72 h. Tissues were subsequently embedded and frozen in OCT (Surgipath FSC22, Leica Microsystems, Wetzlar, Germany). The lumbar segments of spinal cords were cut at 50 μm using a cryostat (Leica Microsystems). Sections were then mounted on gelatinized slides and stored at −20 °C.

Spinal cord sections form Fast Blue-injected mice were imaged directly. Sections from RV-G pseudotyped lentiviral vector-injected mice underwent a further staining step to enhance the signal. Immunohistochemistry was performed on slide-mounted spinal cord sections. Tissue was permeabilized for 1 h with PBS containing 10% donkey serum and 0.1% Triton X-100. Antibody to eGFP (ab290, Abcam; 1:500) was diluted in the same buffer and placed on sections overnight at 4 °C. Sections were then blocked for 30 min prior to incubating for 3 h at room tem; 1:400). Sections were coverslipped with ProLong antifade aqueous mounting medium (Invitrogen) containing DAPI (Sigma-Aldrich; 1:2,000). Immunostained and Fast Blue-

containing sections were imaged using a Leica SP5 II confocal microscope and processed using ImageJ software.

Fixed Imaging of Motor Neurons—Neurons were treated as described in figure legends, fixed in 4% PFA, and then quenched in PBS with 100 mM glycine before permeabilization in PBS plus 2% BSA and 0.1% Triton X-100 and addition of primary antibodies. Staining was visualized using Alexa Fluor secondary antibodies (Invitrogen). Cells were then imaged using a Leica SP5 II confocal microscope and processed using ImageJ, and images were enhanced using a 1.0-pixel median filter and brightness/contrast and then rendered and pseudocolored using Adobe Photoshop.

Colocalization of signals was quantified as reported previously (23, 25) by identifying double positive structures defined on the basis of the following criteria. 1) The compartment is labeled in two different channels and there is overlap of the signals in the merged image. 2) The morphology of the compartment is similar in the two channels. For the Rab studies (Fig. 4), partial overlap was also considered as colocalization as endosomes co-distribute (form Rab5/7-positive patches) during early to late transition (35).

Live Imaging of Lentiviral Trafficking—Imaging of NSC-34 cells was carried out as described previously (33). Briefly, NSC-34 cells were plated at 10,000 cells/Mattek dish previously coated with 100 μg/ml poly-D-lysine (Sigma), 10 μg/ml laminin (Sigma), and 10 μg/ml fibronectin adhesion-promoting peptide (Sigma), and differentiation was induced 24 h after plating. Primary motor neuron cultures were prepared as above and plated onto poly-L-ornithine- and laminin-coated Mattek dishes at a density of 50,000 cells/cm^2. Live imaging was performed as described (25). Briefly, cells were incubated with labeled lentiviral particles at multiplicity of infection (m.o.i.) 10 for 30 min with or without Alexa Fluor 647-labeled anti-p75^{NTR} before cells were washed and fresh medium was added. Dishes were then imaged using a Leica SP5 II confocal microscope with an environmental chamber. Images were taken every 5 s using either the 488 nm laser line (Vybrant DiO and FlAsH) or the 633 nm laser line (Vybrant DiD or Alexa Fluor 647) with a photomultiplier tube detection range of 500–550 nm (Vybrant DiO and FlAsH) or 660–800 nm (Vybrant DiD or Alexa Fluor 647). Images were processed using ImageJ and enhanced using a 1.0-pixel median filter and brightness/contrast. Because of the short distance movements of particles associated with cells (but not necessarily inside cells), analysis was restricted to particles moving >20 μm in a single direction. Particle analysis was performed using MTrackJ and multiple Kymograph ImageJ plugins. Fixed images and kymographs were then rendered and pseudocolored using Adobe Photoshop.

Imaging in Microfluidic Chambers—Motor neurons were purified as above and plated at 200,000 cells/dish into microfluidic chambers (27). Seven days postplating, an excess of viral particles (~10,000) was added to the axonal chamber with or without Alexa Fluor 647-labeled anti-p75^{NTR} and incubated for 20 min at 37 °C before the chamber was filled with Neurobasal medium and left for a further 40 min before imaging. For fixed cell imaging, vector particles (with or without antibodies or labeled TeNT H_c) were added to the axonal chamber in 8 μl for 20 min before the chambers were filled with complete Neurobasal medium and left for a total of 2 h to allow retrograde trafficking to occur. Neurons were fixed in 4% PFA, stained, and processed as above. For acidic endosome labeling, imaging was performed as described above. Briefly, LysoTracker DND (Invitrogen) was diluted 1:100,000 and added to both axonal and somatic chambers in 10 μl for 2 h. Then vector particles with Alexa Fluor 647-labeled anti-p75^{NTR} were added to axonal chambers in 8 μl for 20 min before the chambers were filled with complete Neurobasal medium and left for a total of 2 h to allow retrograde trafficking to occur. Neurons were fixed in 4% PFA, stained, and processed as above.

For transduction of motor neurons, DiD-labeled and nonlabeled eGFP-expressing vector particles (2.9×10^6 transducing units approximating m.o.i. 10) were added to either the axonal chamber or the somatic chamber in 8 μl for 20 min before chambers were filled with complete Neurobasal medium and left for a total of 6 h to allow transduction to take place. Medium was then replaced. 72 h post-transduction neurons were fixed in 4% PFA, stained with antibodies against eGFP and SMI32, and processed as above.

TABLE 1
Biological titers of vectors used

Various vectors were produced according to the described methods. Biological titer was determined by serial dilution of vectors in HEK293T cells. The number of cells expressing β-galactosidase was determined 48 h post-transduction by manual counting. LFU, LacZ-forming units.

Vector	Biological titer (mean ± S.E.)
	LFU/ml
RV-G.HIV-1	$3.59 \pm 0.97 \times 10^7$
RV-G.HIV1-DiO	$5.1 \pm 2.11 \times 10^7$
RV-G.HIV1-DiD	$7.4 \pm 1.87 \times 10^7$
RV-G.HIV1-IN-GFP	$1.1 \pm 0.4 \times 10^6$
RV-G.HIV-1 (FlAsH)	$2.29 \pm 0.91 \times 10^7$
RV-G.HIV1-Cys_4-MA-C (FlAsH)	$1.72 \pm 0.38 \times 10^7$
VSV-G.HIV-1	$8.59 \pm 3.4 \times 10^7$
RV-G.EIAV-Cys_4-MA-C (FlAsH)	$9.47 \pm 0.13 \times 10^6$

RESULTS

Production of Fluorescently Labeled Differentially Tagged Lentiviral Vectors—To identify the mechanism of lentiviral retrograde transduction and trafficking by microscopic analysis, we labeled lentiviral vector particles by three independent approaches. The first method was to label the viral envelope with the lipid dye Vybrant DiO or Vybrant DiD. This was achieved by loading the production cells with dye following transfection (see "Experimental Procedures"). This protocol led to efficient labeling of vectors without apparent loss of biological titer (Table 1).

As a second method of labeling, we chose to genetically modify the major structural proteins of the virus using the small Cys_4 tag in combination with the biarsenical dye FlAsH (36, 37). The inserted sequence is significantly smaller than other fluorescent markers (*e.g.* eGFP) and allows efficient fluorescent labeling with minimal impact on the structure and function of the tagged protein (38, 39). For both HIV-1 and EIAV vectors, the capsid, matrix, and nucleocapsid structural proteins are encoded by the *gag* gene (Fig. 1, *A* and *B*). Bioinformatics analysis of Gag protein sequences from all lentiviral genomes revealed the highly variable nature of these viruses and identified regions of conservation and regions of variability within

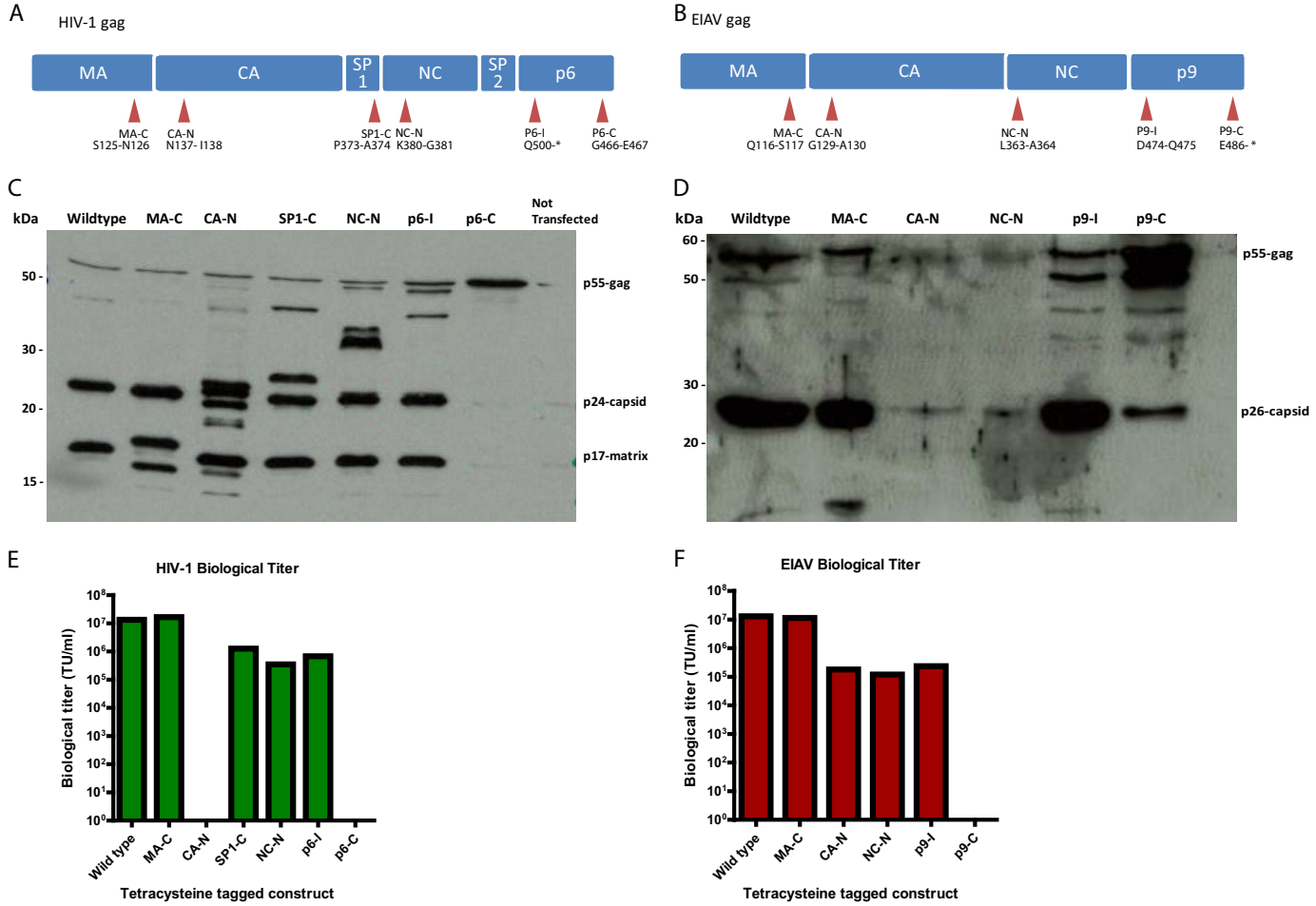

FIGURE 1. **Insertion of tetracysteine tag in the matrix protein allows normal processing of Gag and production of high titer lentiviral vectors.** Diagrammatic representation of HIV-1 Gag (*A*) and EIAV Gag (*B*) and the positions of insertion of the tetracysteine tag. The tags were inserted in regions of variability as deduced from multiple sequence alignment of all primate lentivirus *gag*. *CA*, capsid; *CA-N*, capsid N terminal; *NC*, nucleocapsid; *NC-N*, nucleocapsid N terminal. *C* and *E*, vector-associated Gag was detected by Western blot using anti-HIV-1 Gag and -EIAV Gag antibodies showing the effect of the tetracysteine tag on the efficiency of Gag processing by proteases in HIV-1 (*C*) and EIAV (*E*). *D* and *F*, vector samples were used to transduce 293T cells. The transduced cells were harvested and fixed 72 h after the addition of vectors, and transduction levels were measured by FACS to generate biological titers of the different HIV-1 (*D*) and EIAV (*F*) tagged constructs. *TU*, transducing units.

these sequences. We hypothesized that the regions of variability would be more amenable to the insertion of the Cys_4 tag than regions of conservation. Based on this, the tetracysteine tag was introduced at six and five different locations on HIV-1 *gag* and EIAV *gag*, respectively (Fig. 1, *A* and *B*). We then produced vectors using these tagged constructs (including a wild-type control) and labeled them by loading the FlAsH dye onto the virions post-transfection under mild reducing/binding conditions and removing free dye by sucrose cushion centrifugation (see "Experimental Procedures"). For the HIV-1 constructs, MA-C (Fig. 1*A*) was the only construct that produced biological titers similar to the wild-type, whereas CA-N and p6-C did not have a significant biological titer (Fig. 1*E*). Western blot analysis of the vector particles revealed that the presence of the tetracysteine tag near the termini of individual domains appears to affect the processing efficiency of the nearby proteolytic sites (Fig. 1*C*). p6-C tagging completely prevents proteolytic cleavage, which would explain its inability to transduce and thus lack of a biological titer (Fig. 1*C*). Similarly, for the EIAV constructs, MA-C was again the only construct that produced a significant biological titer comparable with the wild type (Fig. 1*F*). A Western blot analysis of vector particles revealed that the Gag p55 precursor protein containing the Cys_4 tag in the MA-C region underwent proteolytic cleavage in a manner similar to the wild type (Fig. 1*D*). The presence of the tag in other domains appears to affect the processing efficiency of the nearest proteolytic site. This would explain the low biological titers obtained with some of these Gag constructs.

As a third approach, we chose to genetically label components of the viral preintegration complex by fusing eGFP in-frame with the integrase protein, the product of the *pol* gene. This has been achieved previously for HIV-1 integrase with only a modest reduction in titer (40). Accordingly, a C-terminal fusion of integrase-eGFP (IN-eGFP) was made (see "Experimental Procedures") and used to generate RV-G pseudotyped lentiviral particles. Although a reduction in biological titer was observed (Table 1), we still were able to produce a sufficient quantity of transducing virions for investigation.

Characterization of Retrograde Vectors Trafficking in NSC-34 Cells—As a first attempt to determine the retrograde trafficking of lentiviral vectors, we chose to utilize the mouse neuroblastoma/motor neuron cell line NSC-34 (41). These cells can be

differentiated to form axon-like processes by culturing in low serum and have been used previously to demonstrate retrograde trafficking of lentiviral particles pseudotyped with Venezuelan equine encephalitis virus glycoprotein (33). About 70% of NSC-34 cells became differentiated under our culture conditions as judged by the growth of neurites and appeared morphologically healthy, displaying several neuronal markers including neurofilament-200, NCAM, nicotinic acetylcholine receptor, and $p75^{NTR}$ and upon differentiation only metabotropic glutamate receptors 2 and 3 as determined previously by immunocytochemistry and Western blot analysis (41) (data not shown). Differentiated NSC-34 cells were incubated with HIV-1 lentiviral particles containing lipid dye and pseudotyped with RV-G (RV-G.HIV-1-DiO) for 30 min (m.o.i. 10) before imaging by time lapse confocal microscopy. We first observed that several particles were associated with the cells but were not mobile (Fig. 2*A*, *asterisks* (*)). We were unable to determine whether these particles were non-productive viral vectors associated with the outside of the cell or endocytosed vector particles that were unable to undergo or had become stuck during transport. Interestingly, a large number of particles showed appreciable displacement from their point of origin (Fig. 2, *A*, *circles*, and *B*, kymograph, and supplemental Movie 1). These puncta varied in both the distance and speed traveled (compare *red* with *yellow circles*), and tracking analysis revealed that the majority of them traveled in the retrograde direction (Fig. 2*C*). The average speed of individual movements was ~0.2 μm/s; however, over 10% of all measured movements were faster than 0.8 μm/s suggestive of microtubule-mediated transport (Fig. 2*D*). As a production control, HEK293 cells not producing any vector particles were incubated with DiD, and the medium was harvested and concentrated in a manner identical to that for cells producing DiD-labeled vector particles. This purified material was placed onto cells in an identical manner. Although some fluorescent particles were observed floating in the medium (likely labeled cell debris or exosomes), none appeared to bind to or move along axons (data not shown). Thus, the particles observed associated with the cells are highly likely to be labeled lentiviral particles.

These results demonstrated that both Venezuelan equine encephalitis virus glycoprotein (33) and RV-G pseudotyped HIV-1-based lentiviral particles undergo retrograde transport; however, it is possible that this is a property of the HIV-1 capsid rather than the pseudotyping by the glycoprotein. To test this hypothesis, we imaged DiD-labeled HIV-1 lentiviral vectors pseudotyped with VSV-G that do not induce retrograde transduction *in vivo* (4). Although a large number of vectors were observed within the axon-like structures of NSC-34 cells, very few of these showed any displacement from the origin during imaging (only six of 104 vectors). This was in stark contrast to RV-G pseudotyped vectors and suggests that the ability of a vector to undergo retrograde transport is bestowed by RV-G pseudotyping (supplemental Fig. 1).

Because only the envelope of these vectors was labeled, we should exclude the possibility that the tracked signal is derived from vector fused with the limiting membrane of the endosome upon expulsion of the viral capsid (42). To test for this eventuality, we developed vectors with fluorophores in the matrix protein and the capsid itself (see above). Unfortunately, the integrase-eGFP fusion-containing vectors were not sufficiently bright to consistently measure trafficking by time lapse confocal microscopy (not shown). In contrast, the FlAsH-labeled vectors showed intense fluorescence under similar conditions. We then undertook time lapse confocal microscopy experiments as with the Vybrant DiD-labeled vectors (supplemental Fig. 2, A–D). No vectors were observed with wild-type receptors labeled with the FlAsH reagent, demonstrating specificity

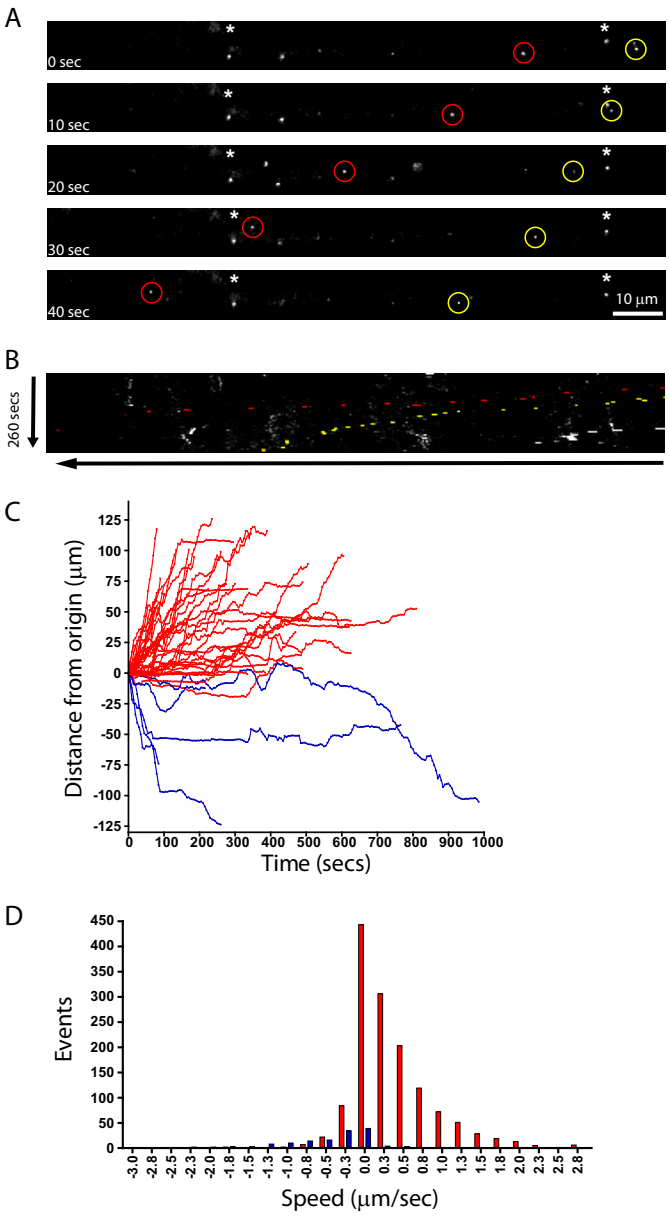

FIGURE 2. **Trafficking of RV-G pseudotyped lentiviral vectors in NSC-34 cells.** Differentiated NSC-34 cells were incubated with RV-G pseudotyped HIV-1 particles labeled with Vybrant DiD for 10 min (m.o.i. 10) prior to imaging. *A*, representative time series from supplemental Movie 1 showing retrograde trafficking particles (*red* and *yellow circles*; cell body is on the *left*). *Asterisks* indicate static particles. *B*, the same time series represented as a kymograph. *C*, single vector analysis showing the displacement from the origin of each particle analyzed (*red*, retrograde trafficking particles (38 tracks); *blue*, anterograde trafficking particles (five tracks)). *D*, speed distribution analysis of individual particle movements (speed between frames) (*red*, retrograde tracks (1386 individual events); *blue*, anterograde tracks (141 individual events)).

of labeling of the inserted tetracysteine tag in the matrix protein (not shown). As with the lipid dye-labeled vectors, NSC-34 cells were incubated for 30 min with RV-G pseudotyped HIV-1-MA-C vectors (m.o.i. 10) labeled with FlAsH. Reinforcing the conclusions obtained with the DiD-labeled HIV-1 lentiviral vectors, a substantial number of vector particles were associated with the axons of these cells but were stationary. For the purposes of displacement and speed measurements, these puncta were excluded from the analysis. A further group of vectors can be seen trafficking along the axons (supplemental Fig. 2, A, circles, and B, kymograph, and supplemental Movie 2). This movement was mainly in the retrograde direction with intermittent back and forth displacement possibly due to the incomplete microtubule polarization in NSC-34 neurites. As for the lipid-labeled vectors, these particles showed considerable variation in terms of speed and distance traveled (supplemental Fig. 2, C and D). The most frequent speed of events was between 0.0 and 0.2 μm/s, reflecting the discontinuous nature of the movement. However, we also observed fast vector trafficking with speeds up to 1.2 μm/s.

Characterization of Retrograde Vector Trafficking in Primary Motor Neurons—Having established that RV-G pseudotyped vectors have a capacity to undergo retrograde transport, we next investigated their trafficking in primary motor neuron cultures. Motor neurons in our cultures were morphologically healthy and co-expressed motor neuron markers Islet-1, SMI32, and calcitonin gene-related peptide as determined by immunocytochemistry (data not shown). First of all we wanted to test whether these vectors are actively internalized, a process that is temperature-dependent. Therefore, we incubated RV-G pseudotyped HIV-1-MA-C-FlAsH vectors with motor neurons on ice to allow the vectors to bind but not undergo endocytosis. Unbound vectors were washed off, and half the cultures were fixed at 4 °C, whereas the remaining dishes were incubated at 37 °C for 45 min before fixation. Both cultures were then stained with an antibody against the RV-G without permeabilization to specifically detect surface-bound vectors. Analysis by confocal microscopy and subsequent quantification revealed that ~75% of the vectors remained bound to the cell surface at 4 °C as indicated by colocalization of the FlAsH and anti-RV-G signals (Fig. 3, *A* and *B*). Cultures incubated at 37 °C showed a large decrease in the colocalized signal, suggesting that these vectors were no longer on the surface. Thus, the entry of these vectors is temperature-dependent, which is indicative of uptake via endocytosis.

We next tested whether retrograde trafficking of RV-G pseudotyped HIV-1 vectors also occurs in primary motor neurons. Time lapse confocal microscopy revealed many RV-G pseudotyped HIV-1 particles that were either associated with the outside of the neuron or internalized into compartments that did not undergo significant displacement (Fig. 3*C*, *asterisks*). This made visualization of trafficking vectors difficult; however, we were still able to observe several vectors that underwent significant displacement along the axon (Fig. 3, *C* and *D*, and supplemental Movie 3). Kinetic analysis of these vectors demonstrated that they were able to undergo extensive displacement, often over 100 μm (Fig. 3*E*). Analysis of these vectors demonstrated that they were able to undergo extensive speed distribution as the curve of these particles is formed by three distinct Gaussian distributions centered at 0.6, 1.8, and 2.8 μm/s (Fig. 3*F*). This compares favorably with that described previously for dynein-mediated retrograde transport (25). Because of intrinsic limitations of the mass culture system of motor neurons (axons tend to grow toward the cell bodies of other neurons, resulting in bundles of antiparallel axons), it is extremely difficult to determine the precise direction of vector trafficking. However, a sustained retrograde movement does seem likely based on the data acquired previously in NSC-34 cells (Fig. 2) and the speeds recorded for other retrogradely transported cargoes (28). Interestingly, comparison of the speed profile of RV-G pseudotyped HIV-1 particle trafficking in NSC-34 cells and motor neurons suggests that both the modal speed and the number of fast events (>2 μm/s) are greater in motor neurons than in NSC-34 cells (supplemental Fig. 3). Additionally, a greater number of pauses (marked by events binned at 0 μm/s in the bar chart in supplemental Fig. 3B) were seen in NSC-34 cells than in motor neurons, a finding likely reflects a more polarized microtubule network in motor neurons. As with NSC-34 cells, data observed when measuring the trafficking of RV-G pseudotyped HIV-1 vectors labeled by FlAsH were similar to data observed for vectors labeled by lipophilic dye (supplemental Fig. 4 and supplemental Movie 4).

Endocytosed cargoes undergo a well characterized journey through distinct early and late endosomal compartments on their way to the lysosome (43). These organelles are characterized by the recruitment of either the small G-protein Rab5 (early endosomes) or Rab7 (late endosomes). To determine whether the trafficking RV-G pseudotyped vectors traverse this pathway, we incubated primary motor neurons with the viral vector for increasing periods of time before fixing and probing the cells for RV-G and either Rab5 or Rab7. As predicted, the RV-G colocalized with both markers; however, colocalization with Rab5 peaked at 10 min after addition of vectors (Fig. 4, *A* and *C*), whereas colocalization with Rab7 continued to increase over time and peaked at 40 – 60 min after addition of the vectors (Fig. 4, *B* and *C*). These data are consistent with the vector entering an endosomal pathway of sequential, transient association with Rab5-positive early endosomes and then accumulation within a Rab7 late endosomal compartment. In contrast to this, HIV-1 vectors pseudotyped with VSV-G showed very little accumulation with either marker at any time point (Fig. 4*D*). This was further confirmed using an anti-p24 antibody (data not shown). This is consistent with the vector fusing with the membrane of the endosome and escaping into the cytosol, which prevents their accumulation in endosomal structures. Because both the RV-G and VSV-G induce fusion at the low pH present in the endosome, what prevents RV-G from initiating fusion and determines its accumulation in the Rab7-positive compartment?

RV-G Pseudotyped HIV-1 Vector Undergoes Retrograde Trafficking in p75^{NTR}-positive Endosomes—Rabies virus is able to enter neuronal cells following interaction with one or more of p75^{NTR}, NCAM, and nAChR (44, 45). Interestingly, p75^{NTR} and NCAM undergo retrograde trafficking in specialized endosomal compartments, which have a luminal neutral pH rather than the acidic pH generally seen in endosomes (30, 46). Thus,

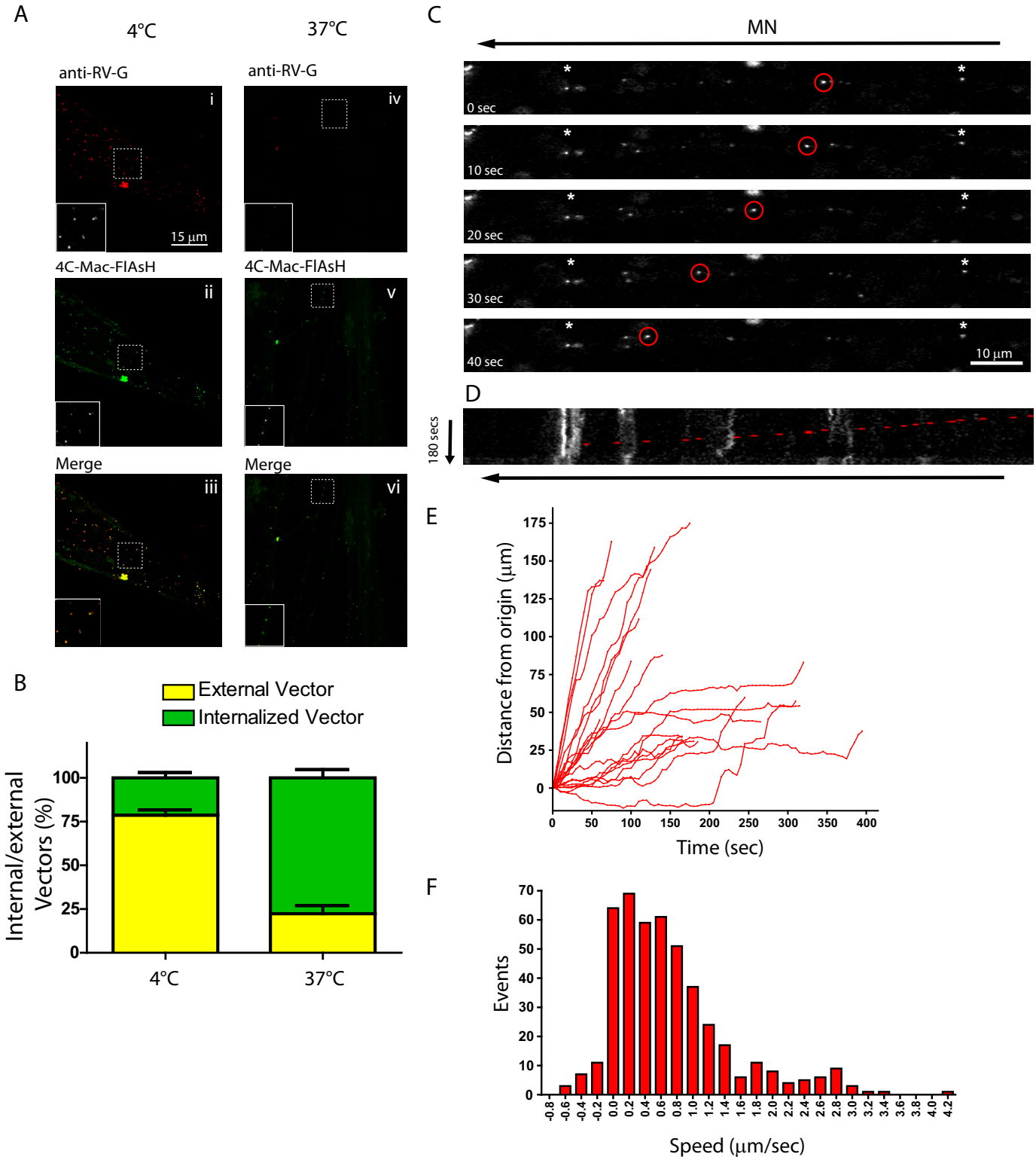

FIGURE 3. **Trafficking of RV-G pseudotyped lentiviral vectors in primary motor neurons.** *A* and *B*, primary motor neurons (DIV 3) were incubated with FlAsH-labeled RV-G pseudotyped HIV-1 vectors (*green*) for 30 min on ice (*panels i–iii*) before placing at 37 °C for 45 min (*panels iv–vi*), fixing under non-permeabilizing conditions, and labeling with anti-RV-G (*red*). Surface vectors are labeled with both markers and appear *yellow* in the merged images (*panels iii* and *vi*), whereas internal vectors are inaccessible to anti RV-G and appear *green*. These data were quantified and expressed as a percentage of total vectors counted (*B*; $n = 3$, 30 cells, 550 particles). *Error bars* represent S.D. *C–F*, motor neurons (DIV 3) were incubated with RV-G pseudotyped HIV-1 vectors (Vybrant DiO- or DiD-labeled) for 30 min (m.o.i. 10) before confocal imaging. *C*, representative image series from supplemental Movie 3. *Asterisks* indicate static particles. *D*, kymograph of the same image series. Individual track analysis (*E*) and speed distribution analysis (*F*) of moving particles (>20 μm in one direction, 20 tracks, 458 individual events) are shown.

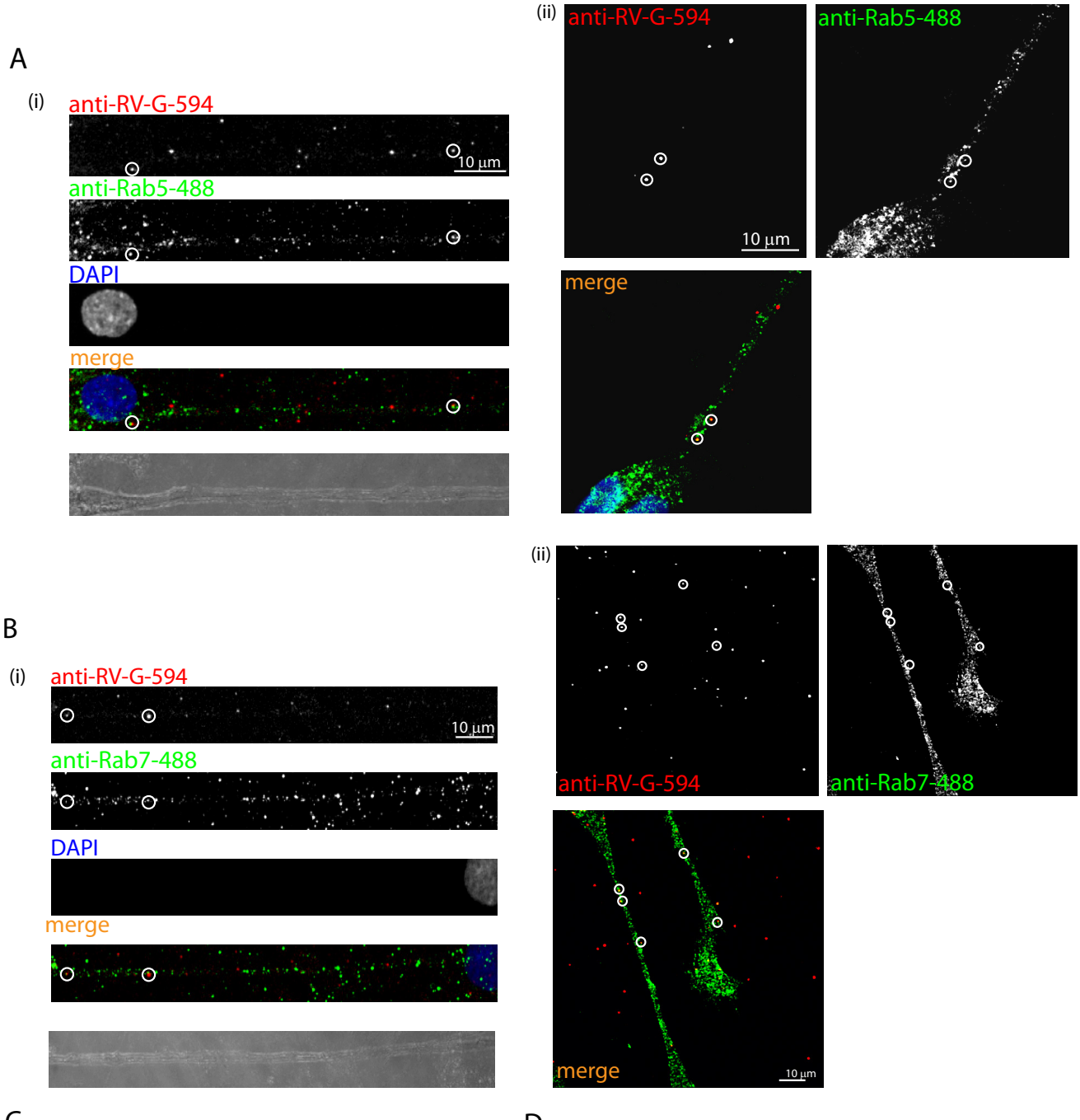
A
(i)
anti-RV-G-594
10 μm
anti-Rab5-488
DAPI
merge
(ii)
anti-RV-G-594
anti-Rab5-488
10 μm
merge
B
(i)
anti-RV-G-594
10 μm
anti-Rab7-488
DAPI
merge
(ii)
anti-RV-G-594
anti-Rab7-488
merge
10 μm
C
Colocalization of RV-G-HIV1 (%)
Rab5
Rab7
***
0
5
10
20
40
60
Time after binding (mins)
D
Colocalization of VSV-G-HIV1 (%)
Rab5
Rab7
0
5
10
20
40
60
Time after binding (mins)

entry into the endosomal pathway would allow trafficking of the viral particles in the absence of endosome fusion driven by acidic pH. To test this hypothesis, we determined whether rabies pseudotyped lentiviral particles undergo endocytosis and subsequent trafficking into the same endosomal pathway. We first demonstrated that we can see good colocalization of RV-G pseudotyped HIV-1 vectors with all three receptors within 5 min of vector addition to the cells. In contrast to the Rab proteins where there is a peak colocalization at 10 min for Rab5 and an accumulation in Rab7 compartments over time, the colocalization with the receptor proteins remained relatively constant throughout the time series (Fig. 5, *A–D*). To further determine whether RV-G pseudotyped HIV-1 vectors undergo axonal retrograde transport, we incubated motor neuron cultures with lipid-labeled vectors and with Alexa Fluor 647-conjugated anti-p75^{NTR} (24, 28). Under these conditions, we could detect multiple p75^{NTR}-positive endosomes undergoing trafficking in the same retrograde direction (Fig. 5, *E*, *panel ii*, and *F*, *panel ii*, and supplemental Movie 5C). Clear examples of RV-G pseudotyped HIV-1 vectors trafficking along the axon were also visible albeit at lower frequency than the p75^{NTR} compartments (Fig. 5, *E*, *panel i*, and *F*, *panel i*, and supplemental Movie 5, A and B). However, these moving viral vectors were consistently within the same endosomal compartment as the p75^{NTR} (Fig. 5, *panel E*, *iii*, and *panel F*, *iii*, and supplemental Movie 5B). This suggests that RV-G pseudotyped HIV-1 does indeed undergo retrograde transport in p75^{NTR}-positive endosomes. Interestingly, we were able to observe many vectors colocalized with p75^{NTR} but not undergoing trafficking (supplemental Fig. 5). This suggests that not all p75^{NTR} endosomes are able to undergo retrograde transport and may explain the apparent rarity of RV-G pseudotyped HIV-1 vector trafficking in mass culture.

Compartmentalized Motor Neuron Cultures Reveal Extensive Retrograde Transport of RV-G Pseudotyped HIV-1 Vector—The endocytic trafficking route taken by the RV-G pseudotyped virions may vary depending upon in which part of the axon the vector undergoes internalization. To test whether this is the case and to unambiguously demonstrate that RV-G pseudotyping does allow retrograde trafficking, we grew motor neurons in microfluidic chambers (MFCs) (27). These inserts allow the creation of compartmented cultures of motor neurons in which neurons project axons though microchannels to a second chamber, allowing separation of somas, axons, and axon terminals. Time lapse imaging following co-application of both RV-G pseudotyped HIV-1 and anti-p75^{NTR} for 60 min showed that fast retrograde transport of RV-G pseudotyped HIV-1 was easily detectable (Fig. 6, *A* and *B*, *panel i*, and supplemental Movie 6A), and as in non-compartmental, *mass* cultures, these were predominantly colocalized with p75^{NTR} (80.25 ± 10% (S.D.); supplemental Movie 6B). In contrast to the data obtained in *mass* cultures, RV-G pseudotyped HIV-1 vector trafficking events were easier to detect (82 particles in 36 microgrooves), suggesting that RV-G pseudotyped HIV-1 transport is quite efficient under these experimental conditions. This result may be due to the decreased background of MFCs or to the increased concentration of vectors at the axon tip. Approximately 85% of the transported vectors colocalized with TeNT H$_c$, and the majority of these also colocalized with p75^{NTR} (Fig. 6, *C* and *D*). Importantly, these data were confirmed when using the RV-G pseudotyped HIV-1 vectors expressing the integrase-eGFP fusion molecule. Although a slightly higher number of vectors not colocalizing with either marker was observed, the majority of RV-G pseudotyped HIV signal could be seen within the same endosomal compartment as the TeNT H$_c$ (Fig. 6, *D* and *E*). It has recently been shown that NCAM undergoes retrograde transport in the same endosomal carriers as p75^{NTR} (30); however, it is not known whether the nAChR also undergoes retrograde trafficking. Using MFC cultures, retrograde transport of the labeled antagonist α-bungarotoxin was clearly observed (supplemental Fig. 6, A and B), and over 50% of the observed endosomes were also positive for TeNT H$_c$ (supplemental Fig. 6, C and D). Interestingly, 40% of the observed DiO-labeled RV-G pseudotyped HIV-1 particles colocalized with both α-bungarotoxin and TeNT H$_c$. It has previously been demonstrated that TeNT H$_c$, p75^{NTR}, and NCAM undergo trafficking in pH-neutral endosomes (22, 30, 46), and we hypothesize that this neutral environment prevents viral fusion and escape. To verify that the endosomal transport compartment used by RV-G pseudotyped HIV-1 vectors is also pH-neutral, motor neurons were incubated with the acidotropic probe LysoTracker DND for 2 h to label the acidic compartments before addition of RV-G pseudotyped HIV-1 DiO-labeled vectors for 2 h. Under these conditions, only 12% of all particles were positive for LysoTracker, and even when restricted to vectors that colocalize with p75^{NTR} (endosomal), only 20.74% of particles can be found in acidic compartments (Fig. 6, *F* and *G*). These data reveal that RV-G pseudotyped HIV-1 vectors are able to undergo axonal retrograde transport in signaling endosomes in primary motor neurons (47).

Despite observing extensive retrograde trafficking of RV-G pseudotyped HIV-1 vectors, we were only able to observe retrograde transduction on rare occasions (*i.e.* neurons transduced following application of vectors to the axonal compartment of MFCs; supplemental Fig. 8). This contrasts dramatically with the efficient transduction seen when the same vectors were added directly to mass culture or when applied to the somatic compartment of MFCs (supplemental Fig. 7A). Thus, despite these vectors being competent for transduction and able to undergo efficient retrograde transport, retrograde *transduction* remains an inefficient process.

To further test the retrograde transduction efficiency of these RV-G HIV-1 vectors *in vivo*, we injected them in the right gastrocnemius muscle of mice and assessed eGFP

FIGURE 4. **RV-G pseudotyped HIV-1 vectors enter a sequential Rab5 and Rab7 endocytic pathway.** Primary motor neurons (DIV3) were incubated with RV-G pseudotyped HIV-1 vectors (*A* and *B*) for 10 min and then incubated at 37 °C for the indicated times before fixing and staining with anti-RV-G (*A* and *B*, *red*) and either anti-Rab5 (*A*, *green*) or anti-Rab7 (*B*, *green*). *A* and *B* show representative examples of colocalization (*circles*) after 10 (*A*, *panels i* and *ii*) or 40 min (*B*, *panels i* and *ii*). Vector colocalization was then quantified and expressed as a percentage of total vectors (*C*; $n = 3$, 15–20 vectors per time point; ***, $p > 0.001$, two-way analysis of variance). Similar experiments were performed with VSV-G pseudotyped HIV-1 vectors, and the data were quantified using anti-VSV-G (*D*). *Error bars* represent S.D.

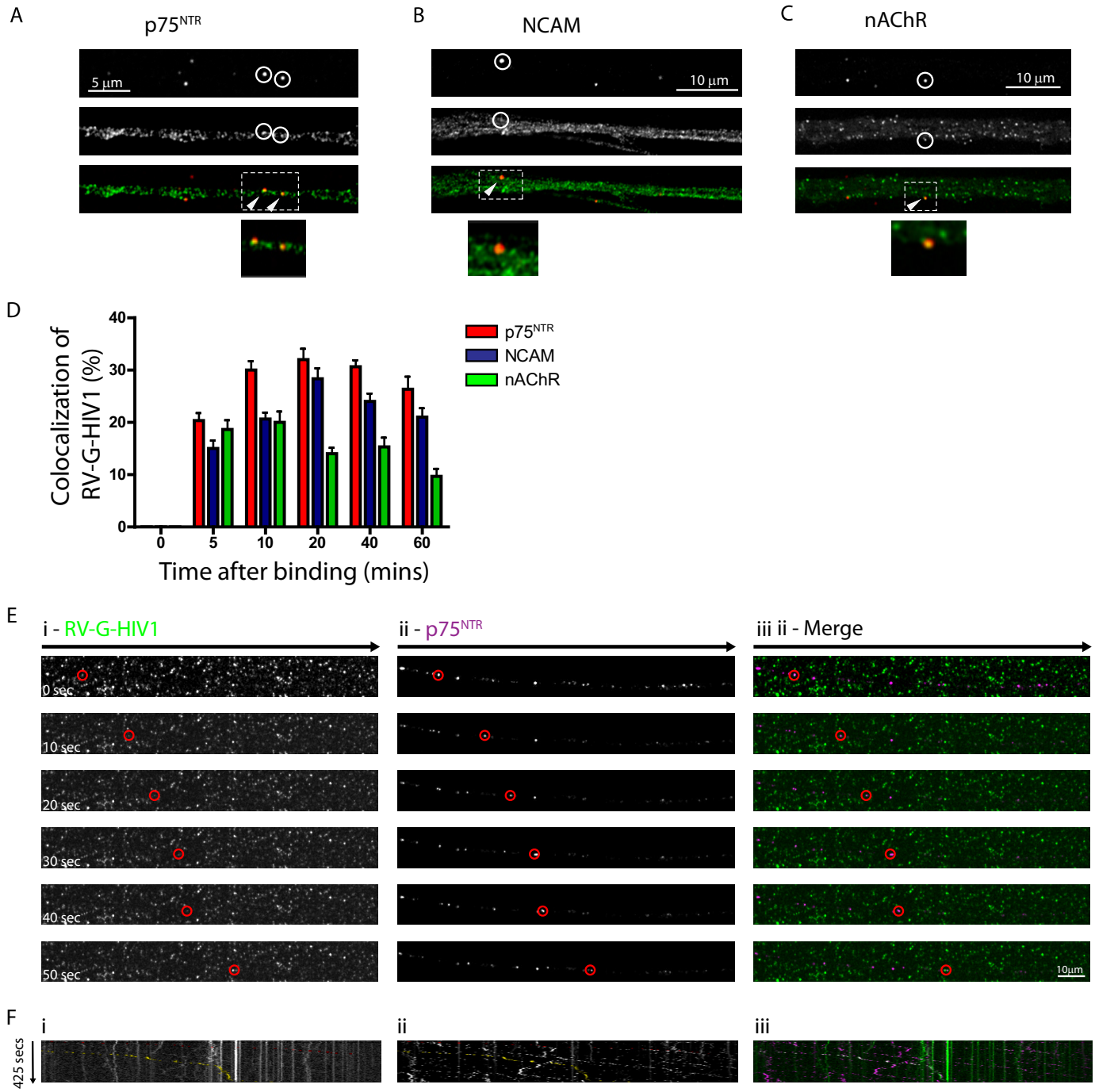

FIGURE 5. **Endocytosed RV-G pseudotyped lentiviral vectors colocalize with the cognate receptors for rabies virus and cotraffic within the same compartment.** *A–D*, primary motor neurons (DIV3) were incubated with RV-G pseudotyped HIV-1 vectors (*A–C*) for 10 min and then incubated at 37 °C for the indicated times before fixing and staining. Colocalization with the indicated receptors was quantified and then expressed as a percentage of total vectors detected (*D*; $n = 3$, 15–20 particles per time point). *Error bars* represent S.D. Shown are representative images of anti-RV-G (*A–C*, *red*) and either anti-p75^{NTR} (*A*, *green*), anti-NCAM (*B*, *green*), or anti-nAChR (*C*, *green*). The segment denoted by a *white rectangle* is enlarged below to show colocalization in the axon. *E* and *F*, motor neurons (DIV 3) were incubated with RV-G pseudotyped HIV-1 vectors (Vybrant DiO-labeled) and anti-p75^{NTR}-Alexa Fluor 647 for 30 min (m.o.i. 10) before time lapse confocal imaging. *E*, representative image series of trafficking vector particles from supplemental Movie 5 showing RV-G pseudotyped HIV-1 (*panel i*; *green* in merged image in *panel iii*) and p75^{NTR} (*panel ii*; *magenta* in merged image in *panel iii*). *F*, kymographs of the same image series.

expression in lumbar motor neurons 3 weeks postinjection as a percentage of Fast Blue retrograde traced motor neurons resulting from similar injections. We only detected transduction of 13 ± 9.6% of retrograde labeled motor neurons (supplemental Fig. 9), which compares well with the low retrograde transduction efficiency observed in previous studies with HIV-1 vectors of identical pseudotype using this route (48). EIAV vectors pseudotyped with a different RV-G Evelyn Rokitnicki Abelseth strain (ERA) result in 27% transduction of lumbar motor neurons back-labeled with FluoroGold following injection of 5 times the volume in the rat (4). Taken together, these data suggest that the reduced efficiency of transduction observed *in vivo* may be

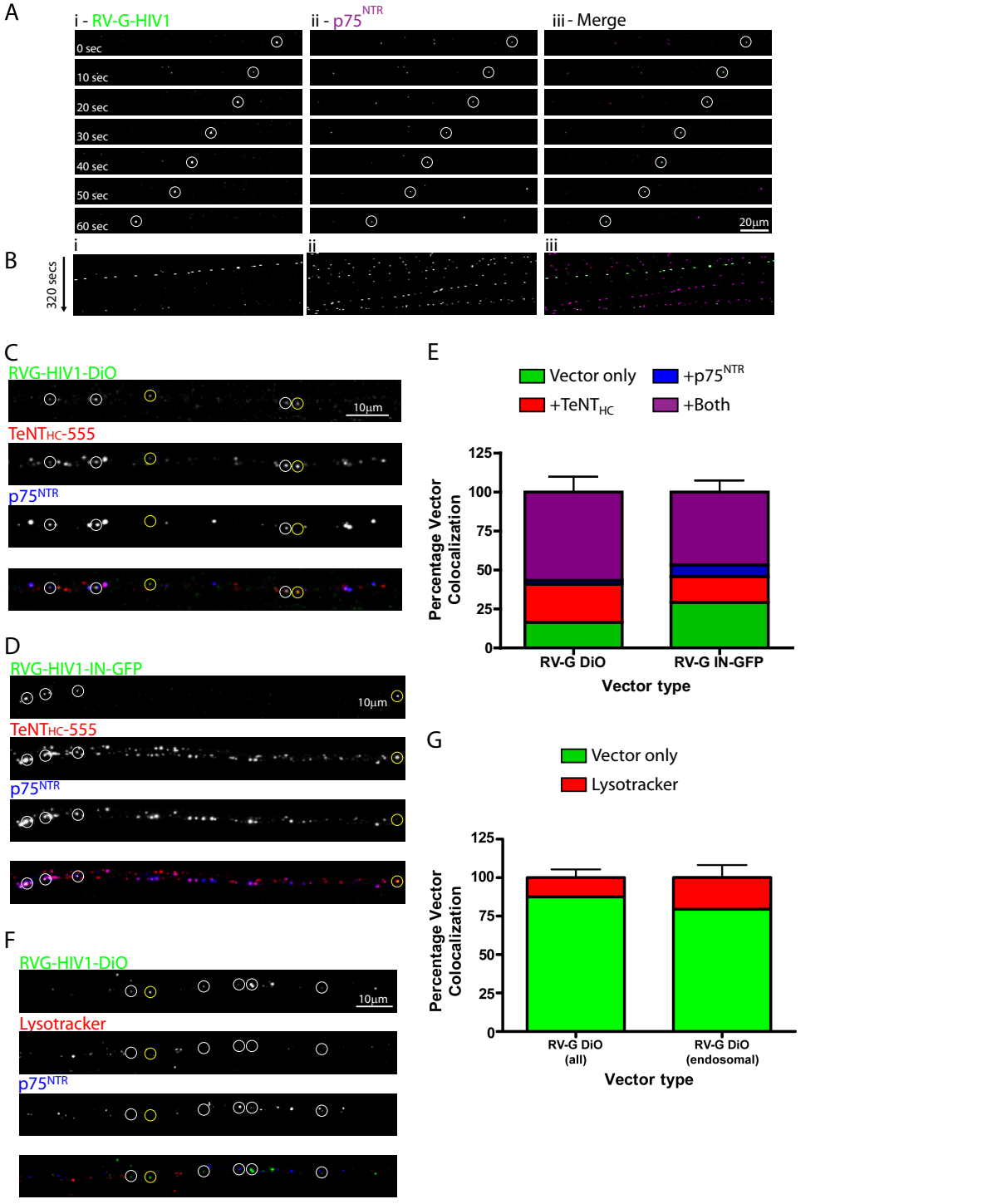

FIGURE 6. **Retrograde trafficking of RV-G pseudotyped lentiviral vectors in compartmented primary motor neuron cultures.** *A* and *B*, primary motor neurons plated in microfluidic chambers (DIV 7) were incubated with RV-G pseudotyped HIV-1 vectors (Vybrant DiO-labeled) and anti-p75^{NTR}-Alexa Fluor 647 for 60 min in the axonal chamber before time lapse confocal imaging of a region of axon >200 μm or more from the axonal compartment. *A*, representative image series of trafficking vector particles from supplemental Movie 6 showing RV-G pseudotyped HIV-1 (*panel i*; green in merged image in *panel iii*) and p75^{NTR} (*panel ii*; *magenta* in merged image in *panel iii*). *B*, kymographs of the same image series. *C–E*, motor neurons (DIV 7) grown in microfluidic chambers were incubated with either DiO-labeled RV-G pseudotyped HIV-1 (*C*) or RV-G-HIV1-IN-eGFP (*D*) with TeNT-Alexa Fluor 555 and anti-p75^{NTR}-Alexa Fluor 647 for 2 h at 37 °C before fixing and imaging by confocal microscopy. Shown are representative maximum projections of Z-stack images (*C* and *D*) where *white circles* show examples of colocalization of vectors with both markers and *yellow circles* show examples of colocalization with just TeNT H_c-Alexa Fluor 555. *E* shows quantification of colocalization ($n = 3$, 172 RV-G pseudotyped DiO-labeled vector particles, 101 RV-G pseudotyped IN-eGFP vector particles). *Error bars* represent S.D. *F* and *G*, motor neurons (DIV 7) were grown in microfluidic chambers and incubated with LysoTracker DND (10 nM) for 2 h followed by DiO-labeled RV-G pseudotyped HIV-1 and anti-p75^{NTR}-Alexa Fluor 647 for 2 h at 37 °C before fixing and imaging by confocal microscopy. Shown is a representative maximum projection of Z-stack images (*F*) where *white circles* show examples of vectors with p75^{NTR} alone and *yellow circles* show examples of colocalization with LysoTracker. *G* shows quantification of colocalization of all vectors or of vectors within endosomes that are either p75^{NTR}- and/or LysoTracker-positive ($n = 3$, 127 particles or 78 particles, respectively). *Error bars* represent S.D.

a reflection of processes post-trafficking rather than purely an inefficiency of vector uptake and identify the existence of a post-transport barrier to transduction when using the retrograde route.

RV-G Pseudotyping Confers Retrograde Axonal Trafficking on EIAV Vectors—Although multiple lines of evidence suggest that RV-G pseudotyping can target HIV-1 vectors for retrograde axonal transport, it is formally possible for this process to be mediated by the HIV-1 core rather than the pseudotyped glycoprotein. To test for this possibility, a tetracysteine tag was inserted into the matrix protein of the EIAV viral *gag* gene (see "Experimental Procedures" and Fig. 1, *D–F*). Vectors were then produced and labeled with the biarsenical dye FlAsH as described previously. These vectors were then added to motor neurons grown in mass culture in the presence of labeled antibodies against $p75^{NTR}$. As with RV-G pseudotyped HIV-1 vectors, RV-G pseudotyped EIAV vectors were clearly observed to undergo axonal transport mostly within endosomal compartments positive for $p75^{NTR}$ (Fig. 7, *A–C*, and supplemental Movie 7).

Taken together, we demonstrated that pseudotyping lentiviral particles with RV-G conferred the ability to the vector to enter the retrograde transport compartment in motor neuron axons irrespective of the lentiviral vector particle used. Furthermore, we demonstrated that this process was mediated by the recruitment of the vector to $p75^{NTR}$-positive endosomal compartments. These data explain how RV-G pseudotyped lentiviral vectors are able to transduce spinal motor neurons even after distal intramuscular application of vectors *in vivo* (4, 48).

DISCUSSION

Lentiviral particles are highly promising delivery vectors for gene therapy, and pseudotyping these vectors with specific viral glycoproteins allows them to be targeted to specific cell populations. Pseudotyping with glycoprotein from the rabies virus produces vectors that are more neurotropic and allows neuronal transduction even when delivered to distal sites (retrograde transduction) (4). This development makes RV-G pseudotyped vectors an attractive vector for gene therapy of motor neuron diseases because vectors can be delivered to the motor neurons simply by intramuscular injection without the requirement for invasive intraspinal injection (49). Currently, it is unknown what molecular processes underlie this retrograde transduction. Here, we investigated how retrograde transduction may occur and demonstrated that RV-G pseudotyping conferred retrograde trafficking on two different lentiviral vectors, and this trafficking was mediated through an interaction with either of the cognate RV-G receptors and via a Rab7-positive endosomal compartment.

Studying trafficking of mature HIV-1 or EIAV particles has been a difficult process primarily because insertion of traditional tags such as eGFP into the viral capsid has resulted in significantly reduced vector production (38). Here, we utilized a number of complimentary labeling techniques to visualize receptor trafficking. Labeling of the envelope with lipophilic dyes allowed highly efficient labeling of viral vectors; however, it is possible that the dye would stay within the endosome following vector fusion. This phenomenon may in principle generate misleading data, although it is unlikely due to the high

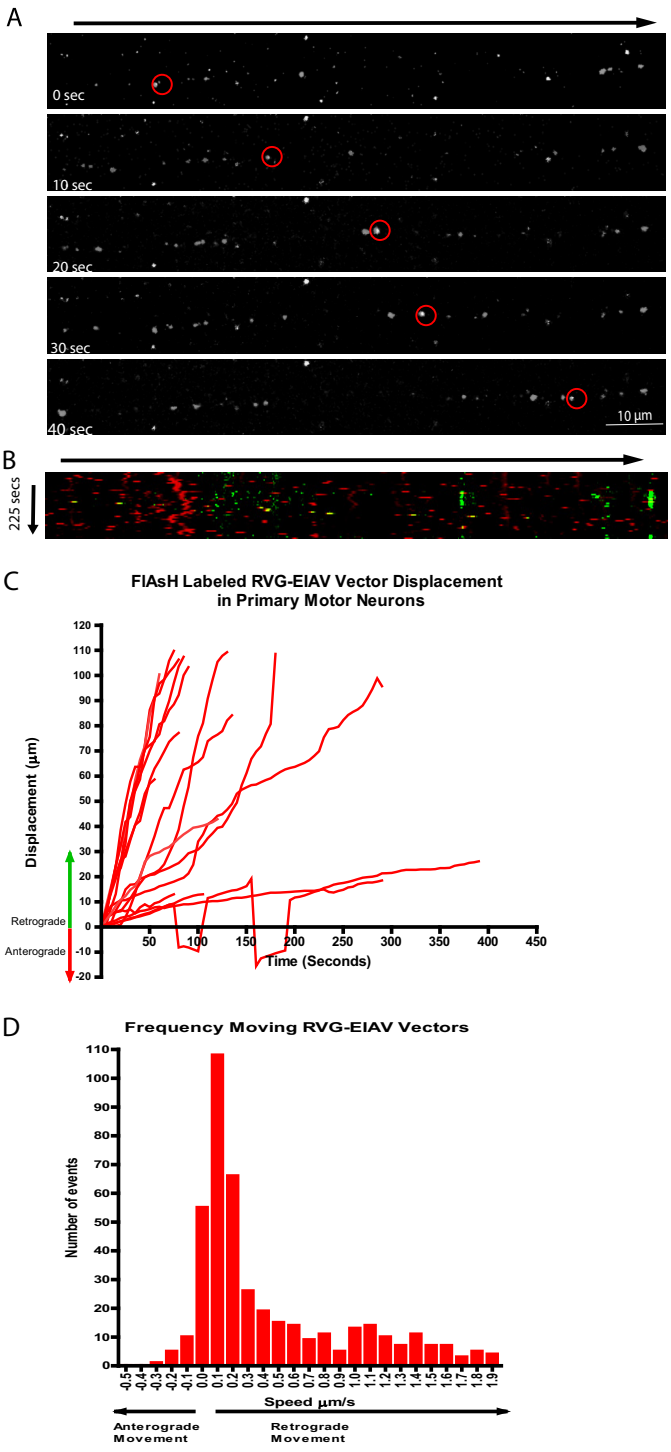

FIGURE 7. **Pseudotyping with RV-G targets EIAV vectors for retrograde endosomal transport in primary motor neuron cultures.** *A* and *B*, primary motor neurons were incubated with FlAsH-labeled RV-G pseudotyped EIAV vectors for 30 min with Alexa Fluor 647-labeled anti-$p75^{NTR}$ antibody before confocal imaging. *A*, representative time series from supplemental Movie 7 showing retrograde trafficking of vector particle (*red circles*; cell body is on the *right*). *B*, kymographs of the same image series (*yellow* spots). *C*, single vector track analysis showing the displacement of each moving particle (16 tracks). *D*, speed distribution analysis of individual particle movements (441 events).

level of membrane turnover in endosomes. To demonstrate that this is not the case, we additionally fluorescently labeled components of the viral capsid itself. We chose to use a small tetracysteine tag and the biarsenical dye FlAsH. We postulated

that this relatively small tag was less likely to impact the biological activity of the vector and carefully selected insertion sites on the structural proteins encoded by the *gag* gene. However, even with this relatively small addition, the tagging of the capsid led to a large reduction in biological titer (Fig. 1, *C* and *F*), thus confirming previous reports showing that insertion of the tetracysteine tag at both the N and C termini of the capsid protein of HIV-1 completely abolished virus infectivity (51). This would suggest that the stability of the highly ordered capsid lattice might be compromised by the tetracysteine tag. Interestingly, insertion of this tag in the EIAV capsid (Fig. 1*F*) did not completely abolish its ability to transduce neurons, indicating that regions of variability in the *gag* sequence are not the only criterion for the successful insertion of the tetracysteine tag.

We were able to add the tag to the matrix protein with minimal reduction in titer in both HIV-1 and EIAV particles (Fig. 1). A major limitation of the biarsenical labeling system is the high degree of background fluorescence often observed (52). We were able to overcome this issue by ultracentrifuging the labeled vector through a sucrose cushion, which resulted in the removal of free, unincorporated biarsenical dye. Results obtained with this strategy will likely prove useful in the study of viral trafficking both for pseudotyped lentiviral particles and wild-type HIV-1 and EIAV vectors. Use of these fluorescent vectors verified the results seen with the lipophilic dye and further demonstrated the validity of our conclusions.

Extensive study in motor neurons has revealed an elegant process by which proteins within the distal portion of the axon can undergo axonal retrograde transport to the soma, a process first identified as a mechanism for allowing extracellular signals at the axon tip to be transmitted to the cell body through retrogradely trafficked signaling endosomes (53). This process has been best characterized for neurotrophin receptors including $p75^{NTR}$ and as with many endosomal processes involves the trafficking of the receptor through Rab5-positive endosomes and accumulation in Rab7-positive endosomes (23). These organelles then undergo microtubule-dependent axonal transport toward the soma that is mainly mediated by the microtubule motor cytoplasmic dynein (20). In addition to $p75^{NTR}$, this pathway has been shown to mediate the transport of cell adhesion molecules (a*ctivated leukocyte cell adhesion molecule* and NCAM) (30) as well as neurotoxins (*i.e.* tetanus and botulinum neurotoxins) (27) and viruses such as canine adenovirus 2 and its receptor, coxsackievirus and adenovirus receptor (25). Here, we show that this axonal trafficking pathway is responsible for the retrograde transport of RV-G pseudotyped lentiviral vectors and by extension is likely to mediate the trafficking of wild-type rabies virus.

The RV-G is targeted to cell membranes by interaction with specific membrane proteins (45). There are currently three membrane proteins known to bind the RV-G. The first of these is nAChR, which has been suggested to act as a receptor for the wild-type rabies virus (54). Two further proteins have also been proposed, NCAM (55) and $p75^{NTR}$ (56). Here, we demonstrated the co-internalization of RV-G pseudotyped lentiviral vectors with the three membrane proteins suggested to mediate its infectivity. Following internalization, the level of colocalization remained fairly constant, suggesting that the vector remains associated with the proteins along the axon. Consistent with endosomal transport, the lentiviral vectors followed a sequential association with Rab5 followed by Rab7 that is indicative of endosomal maturation along the axonal endocytic pathway. The early association of RV-G lentiviral vectors with Rab5-positive early endosomes and then with Rab7-positive late endosomes is similar to that observed for TeNT (23) and *botulinum* neurotoxin (27). It is likely that the Rab7 effectors Rab7-interacting lysosomal protein and oxysterol-binding protein-related protein 1L mediate the recruitment of cytoplasmic dynein motors to endosomes (57), and this may indicate that only vectors undergoing endosome maturation undergo efficient, long range axonal transport.

Importantly, these Rab7-positive endosomes have a non-acidic pH (LysoTracker-negative) in direct contrast to typical Rab7/late endosomes where the luminal pH is considerably more acidic (46). It is likely that the neutral pH is instrumental in the transport of intact lentiviral vectors because an acidic environment would trigger a conformational change in the RV-G, mediating fusion of the viral envelope with the endosome membrane, thus allowing endosomal escape of the viral capsid (12). As such, the neutral environment prevents endosomal escape, allowing transport of the vector to the soma where fusion occurs, and the capsid can enter the nucleus and integrate into the genome. It is interesting to note that although we were able to detect extensive retrograde transport of vectors in both mass and compartmentalized cultures we were able to detect only inefficient transduction of neurons when incubated under the same conditions enabling axonal retrograde transport (supplemental Fig. 8). Although this may be a result of a proportion of the vectors being unable to integrate due to incomplete assembly of the particle, we think this is unlikely because the same vectors are able to efficiently transduce the same neurons when applied directly to the soma (supplemental Fig. 7A). This is similar to data observed previously with Venezuelan equine encephalitis virus glycoprotein pseudotyped HIV vectors (33), which showed retrograde transport in culture but very little retrograde transduction *in vivo*. This suggests that although targeting the vector for efficient axonal retrograde transport is necessary and sufficient for motor neuron transduction (4) other, post-trafficking factors that are also crucial for the efficiency of this process exist and represent an interesting new direction for improving the efficiency of lentivirus-mediated gene therapy. These are likely to include the ability of the envelope to promote fusion when the endosome does reach the soma and the molecular processes allowing the transport of the capsid to the nucleus. It is interesting that wild-type rabies virus is able to efficiently escape the endosome and get transported to the soma. This might be related to the ability of the intact virus to block degradation in the cell. A recent study indicated that RV-G bound to an antibody transfected in a neuroblastoma cell line is targeted via early and late endosomes to lysosomes (58). In addition, lentiviral vector transduction of dendritic cells involved endosomal trafficking, and its efficiency was enhanced by suppressing autophagy (59). Indeed, we have recently reported an increase in retrograde transduction in the brain of lentiviral vectors pseudotyped with a chimeric RV-G bearing a portion of gp41 for its cytoplasmic tail (60). We have

also observed that incorporation of different yet more efficient fusogens (61) in combination with surface-expressed antibodies targeting neuromuscular junction receptors onto the lentiviral vector surface enhances the ability of retrogradely transported vectors to transduce motor neurons within microfluidic motor neuron cultures following axonal chamber application (50). These and other processes will be an interesting area of future studies with the goal of further improving the gene transfer efficiency of lentiviral gene therapy vectors.

In this study, we demonstrated that pseudotyping both the EIAV and HIV-1 lentiviral vectors with the rabies viral glycoprotein targeted these vectors for endocytosis and axonal transport via a $p75^{NTR}$-positive endosomal compartment. This process was both rapid and efficient in primary motor neuron cultures, suggesting that the inherent inefficiency of retrograde transduction likely reflects postendosomal transport mechanisms rather than inability to undergo transport. Our data further demonstrate the importance of this pathway for neuronal homeostasis and how viruses and toxins have evolved to make use of its unique trafficking route.

Acknowledgments—We thank Kinga Bercsenyi, Maciej J. M. Szukszto, and Sultana Mahjabeen Miah for contributing to this project. We also thank Professor Ronald Montelaro (University of Pittsburgh School of Medicine) for providing the p26 EIAV reference serum.

REFERENCES

1. Wong, L.-F., Goodhead, L., Prat, C., Mitrophanous, K. A., Kingsman, S. M., and Mazarakis, N. D. (2006) Lentivirus-mediated gene transfer to the central nervous system: therapeutic and research applications. *Hum. Gene Ther.* **17,** 1–9
2. Sakuma, T., Barry, M. A., and Ikeda, Y. (2012) Lentiviral vectors: basic to translational. *Biochem. J.* **443,** 603–618
3. Cronin, J., Zhang, X.-Y., and Reiser, J. (2005) Altering the tropism of lentiviral vectors through pseudotyping. *Curr. Gene Ther.* **5,** 387–398
4. Mazarakis, N. D., Azzouz, M., Rohll, J. B., Ellard, F. M., Wilkes, F. J., Olsen, A. L., Carter, E. E., Barber, R. D., Baban, D. F., Kingsman, S. M., Kingsman, A. J., O'Malley, K., and Mitrophanous, K. A. (2001) Rabies virus glycoprotein pseudotyping of lentiviral vectors enables retrograde axonal transport and access to the nervous system after peripheral delivery. *Hum. Mol. Genet.* **10,** 2109–2121
5. Azzouz, M., Le, T., Ralph, G. S., Walmsley, L., Monani, U. R., Lee, D. C., Wilkes, F., Mitrophanous, K. A., Kingsman, S. M., Burghes, A. H., and Mazarakis, N. D. (2004) Lentivector-mediated SMN replacement in a mouse model of spinal muscular atrophy. *J. Clin. Investig.* **114,** 1726–1731
6. Ralph, G. S., Radcliffe, P. A., Day, D. M., Carthy, J. M., Leroux, M. A., Lee, D. C., Wong, L.-F., Bilsland, L. G., Greensmith, L., Kingsman, S. M., Mitrophanous, K. A., Mazarakis, N. D., and Azzouz, M. (2005) Silencing mutant SOD1 using RNAi protects against neurodegeneration and extends survival in an ALS model. *Nat. Med.* **11,** 429–433
7. Verhoeyen, E., and Cosset, F.-L. (2004) Surface-engineering of lentiviral vectors. *J. Gene Med.* **6,** Suppl. 1, S83–S94
8. Oksayan, S., Ito, N., Moseley, G., and Blondel, D. (2012) Subcellular trafficking in rhabdovirus infection and immune evasion: a novel target for therapeutics. *Infect. Disord. Drug Targets* **12,** 38–58
9. Miaczynska, M., and Zerial, M. (2002) Mosaic organization of the endocytic pathway. *Exp. Cell Res.* **272,** 8–14
10. Rink, J., Ghigo, E., Kalaidzidis, Y., and Zerial, M. (2005) Rab conversion as a mechanism of progression from early to late endosomes. *Cell* **122,** 735–749
11. Gaudin, Y., Ruigrok, R. W., Knossow, M., and Flamand, A. (1993) Glycoprotein and their role in membrane fusion. Low-pH conformational changes of rabies virus glycoprotein and their role in membrane fusion. *J. Virol.* **67,** 1365–1372
12. Gaudin, Y. (1999) Rabies virus-induced membrane fusion pathway. *Mol. Membr. Biol.* **16,** 21–31
13. Rasalingam, P., Rossiter, J. P., Mebatsion, T., and Jackson, A. C. (2005) Comparative pathogenesis of the SAD-L16 strain of rabies virus and a mutant modifying the dynein light chain binding site of the rabies virus phosphoprotein in young mice. *Virus Res.* **111,** 55–60
14. Raux, H., Flamand, A., and Blondel, D. (2000) Interaction of the rabies virus P protein with the LC8 dynein light chain. *J. Virol.* **74,** 10212–10216
15. Moseley, G. W., Roth, D. M., DeJesus, M. A., Leyton, D. L., Filmer, R. P., Pouton, C. W., and Jans, D. A. (2007) Dynein light chain association sequences can facilitate nuclear protein import. *Mol. Biol. Cell* **18,** 3204–3213
16. Klingen, Y., Conzelmann, K. K., and Finke, S. (2008) Double-labelled rabies virus: live tracking of enveloped virus transport. *J. Virol.* **82,** 237–245
17. Dodding, M. P., and Way, M. (2011) Coupling viruses to dynein and kinesin-1. *EMBO J.* **30,** 3527–3539
18. McDonald, D., Vodicka, M. A., Lucero, G., Svitkina, T. M., Borisy, G. G., Emerman, M., and Hope, T. J. (2002) Visualization of the intracellular behavior of HIV in living cells. *J. Cell Biol.* **159,** 441–452
19. Kovalevich, J., and Langford, D. (2012) Neuronal toxicity in HIV CNS disease. *Future Virol.* **7,** 687–698
20. Salinas, S., Bilsland, L. G., and Schiavo, G. (2008) Molecular landmarks along the axonal route: axonal transport in health and disease. *Curr. Opin. Cell Biol.* **20,** 445–453
21. Salinas, S., Schiavo, G., and Kremer, E. J. (2010) A hitchhiker's guide to the nervous system: the complex journey of viruses and toxins. *Nat. Rev. Microbiol.* **8,** 645–655
22. Lalli, G., and Schiavo, G. (2002) Analysis of retrograde transport in motor neurons reveals common endocytic carriers for tetanus toxin and neurotrophin receptor p75NTR. *J. Cell Biol.* **156,** 233–239
23. Deinhardt, K., Salinas, S., Verastegui, C., Watson, R., Worth, D., Hanrahan, S., Bucci, C., and Schiavo, G. (2006) Rab5 and Rab7 control endocytic sorting along the axonal retrograde transport pathway. *Neuron* **52,** 293–305
24. Deinhardt, K., Reversi, A., Berninghausen, O., Hopkins, C. R., and Schiavo, G. (2007) Neurotrophins redirect p75NTR from a clathrin-independent to a clathrin-dependent endocytic pathway coupled to axonal transport. *Traffic* **8,** 1736–1749
25. Salinas, S., Bilsland, L. G., Henaff, D., Weston, A. E., Keriel, A., Schiavo, G., and Kremer, E. J. (2009) CAR-associated vesicular transport of an adenovirus in motor neuron axons. *PLoS Pathog.* **5,** e1000442
26. Colpitts, T. M., Moore, A. C., Kolokoltsov, A. A., and Davey, R. A. (2007) Venezuelan equine encephalitis virus infection of mosquito cells requires acidification as well as mosquito homologs of the endocytic proteins Rab5 and Rab7. *Virology* **369,** 78–91
27. Restani, L., Giribaldi, F., Manich, M., Bercsenyi, K., Menendez, G., Rossetto, O., Caleo, M., and Schiavo, G. (2012) Botulinum neurotoxins A and E undergo retrograde axonal transport in primary motor neurons. *PLoS Pathog.* **8,** e1003087
28. Deinhardt, K., Berninghausen, O., Willison, H. J., Hopkins, C. R., and Schiavo, G. (2006) Tetanus toxin is internalized by a sequential clathrin-dependent mechanism initiated within lipid microdomains and independent of epsin1. *J. Cell Biol.* **174,** 459–471
29. Butowt, R., and von Bartheld, C. S. (2003) Connecting the dots: trafficking of neurotrophins, lectins and diverse pathogens by binding to the neurotrophin receptor p75NTR. *Eur. J. Neurosci.* **17,** 673–680
30. Wade, A., Thomas, C., Kalmar, B., Terenzio, M., Garin, J., Greensmith, L., and Schiavo, G. (2012) Activated leukocyte cell adhesion molecule modulates neurotrophin signaling. *J. Neurochem.* **121,** 575–586
31. Horton, R. M., Hunt, H. D., Ho, S. N., Pullen, J. K., and Pease, L. R. (1989) Engineering hybrid genes without the use of restriction enzymes: gene splicing by overlap extension. *Gene* **77,** 61–68
32. Warrens, A. N., Jones, M. D., and Lechler, R. I. (1997) Splicing by overlap extension by PCR using asymmetric amplification: an improved technique for the generation of hybrid proteins of immunological interest. *Gene* **186,** 29–35
33. Trabalza, A., Georgiadis, C., Eleftheriadou, I., Hislop, J. N., Ellison, S. M.,

Karavassilis, M. E., and Mazarakis, N. D. (2013) Venezuelan equine encephalitis virus glycoprotein pseudotyping confers neurotropism to lentiviral vectors. *Gene Ther.* **20,** 723–732
34. Carpentier, D. C., Vevis, K., Trabalza, A., Georgiadis, C., Ellison, S. M., Asfahani, R. I., and Mazarakis, N. D. (2012) Enhanced pseudotyping efficiency of HIV-1 lentiviral vectors by a rabies/vesicular stomatitis virus chimeric envelope glycoprotein. *Gene Ther.* **19,** 761–774
35. Spang, A. (2009) On the fate of early endosomes. *Biol. Chem.* **390,** 753–759
36. Griffin, B. A., Adams, S. R., and Tsien, R. Y. (1998) Specific covalent labeling of recombinant protein molecules inside live cells. *Science* **281,** 269–272
37. Adams, S. R., Campbell, R. E., Gross, L. A., Martin, B. R., Walkup, G. K., Yao, Y., Llopis, J., and Tsien, R. Y. (2002) New biarsenical ligands and tetracysteine motifs for protein labeling *in vitro* and *in vivo*: synthesis and biological applications. *J. Am. Chem. Soc.* **124,** 6063–6076
38. Müller, B., Daecke, J., Fackler, O. T., Dittmar, M. T., Zentgraf, H., and Kräusslich, H.-G. (2004) Construction and characterization of a fluorescently labeled infectious human immunodeficiency virus type 1 derivative. *J. Virol.* **78,** 10803–10813
39. Rudner, L., Nydegger, S., Coren, L. V., Nagashima, K., Thali, M., and Ott, D. E. (2005) Dynamic fluorescent imaging of human immunodeficiency virus type 1 gag in live cells by biarsenical labeling. *J. Virol.* **79,** 4055–4065
40. Schenkwein, D., and Turkki, V., Kärkkäinen, H. R., Airenne, K., and Ylä-Herttuala, S. (2010) Production of HIV-1 integrase fusion protein-carrying lentiviral vectors for gene therapy and protein transduction. *Hum. Gene Ther.* **21,** 589–602
41. Cashman, N. R., Durham, H. D., Blusztajn, J. K., Oda, K., Tabira, T., Shaw, I. T., Dahrouge, S., and Antel, J. P. (1992) Neuroblastoma x spinal cord (NSC) hybrid cell lines resemble developing motor neurons. *Dev. Dyn.* **194,** 209–221
42. Padilla-Parra, S., Matos, P. M., Kondo, N., Marin, M., Santos, N. C., and Melikyan, G. B. (2012) Quantitative imaging of endosome acidification and single retrovirus fusion with distinct pools of early endosomes. *Proc. Natl. Acad. Sci. U.S.A.* **109,** 17627–17632
43. Zerial, M., and McBride, H. (2001) Rab proteins as membrane organizers. *Nat. Rev. Mol. Cell Biol.* **2,** 107–117
44. Lafon, M. (2005) Rabies virus receptors. *J. Neurovirol.* **11,** 82–87
45. Schnell, M. J., McGettigan, J. P., Wirblich, C., and Papaneri, A. (2010) The cell biology of rabies virus: using stealth to reach the brain. *Nat. Rev. Microbiol.* **8,** 51–61
46. Bohnert, S., and Schiavo, G. (2005) Tetanus toxin is transported in a novel neuronal compartment characterized by a specialized pH regulation. *J. Biol. Chem.* **280,** 42336–42344
47. Bercsenyi, K., Giribaldi, F., and Schiavo, G. (2013) The elusive compass of clostridial neurotoxins: deciding when and where to go? *Curr. Top. Microbiol. Immunol.* **364,** 91–113
48. Mentis, G. Z., Gravell, M., Hamilton, R., Shneider, N. A., O'Donovan, M. J., and Schubert, M. (2006) Transduction of motor neurons and muscle fibers by intramuscular injection of HIV-1-based vectors pseudotyped with select rabies virus glycoproteins. *J. Neurosci. Methods* **157,** 208–217
49. Azzouz, M., Ralph, G. S., Storkebaum, E., Walmsley, L. E., Mitrophanous, K. A., Kingsman, S. M., Carmeliet, P., and Mazarakis, N. D. (2004) VEGF delivery with retrogradely transported lentivector prolongs survival in a mouse ALS model. *Nature* **429,** 413–417
50. Eleftheriadou, I., Trabalza, A., Ellison, S., Gharun, K., and Mazarakis, N. (2014) Specific retrograde transduction of spinal motor neurons using lentiviral vectors targeted to presynaptic NMJ receptors. *Mol. Ther.* 10.1038/mt.2014.49
51. Campbell, E. M., Perez, O., Anderson, J. L., and Hope, T. J. (2008) Visualization of a proteasome-independent intermediate during restriction of HIV-1 by rhesus TRIM5α. *J. Cell Biol.* **180,** 549–561
52. Stroffekova, K., Proenza, C., and Beam, K. (2001) The protein-labeling reagent FLASH-EDT 2 binds not only to CCXXCC motifs but also non-specifically to endogenous cysteine-rich proteins. *Pflugers Arch.* **442,** 859–866
53. Ginty, D. (2002) Retrograde neurotrophin signaling: Trk-ing along the axon. *Curr. Opin. Neurobiol.* **12,** 268–274
54. Lentz, T. L., Burrage, T. G., Smith, A. L., and Tignor, G. H. (1983) The acetylcholine receptor as a cellular receptor for rabies virus. *Yale J. Biol. Med.* **56,** 315–322
55. Thoulouze, M. I., Lafage, M., Schachner, M., Hartmann, U., Cremer, H., and Lafon, M. (1998) The neural cell adhesion molecule is a receptor for rabies virus. *J. Virol.* **72,** 7181–7190
56. Tuffereau, C., Bénéjean, J., Blondel, D., Kieffer, B., and Flamand, A. (1998) Low-affinity nerve-growth factor receptor (P75NTR) can serve as a receptor for rabies virus. *EMBO J.* **17,** 7250–7259
57. Johansson, M., Rocha, N., Zwart, W., Jordens, I., Janssen, L., Kuijl, C., Olkkonen, V. M., and Neefjes, J. (2007) Activation of endosomal dynein motors by stepwise assembly of Rab7-RILP-p150Glued, ORP1L, and the receptor βIII spectrin. *J. Cell Biol.* **176,** 459–471
58. St Pierre, C. A., Leonard, D., Corvera, S., Kurt-Jones, E. A., and Finberg, R. W. (2011) Antibodies to cell surface proteins redirect intracellular trafficking pathways. *Exp. Mol. Pathol.* **91,** 723–732
59. Liu, Y., Tai A., Joo K. I., and Wang P. (2013) Visualisation of DC-SIGN-mediated entry pathway of engineered lentiviral vectors in target cells. *PLoS One* **8,** e67400
60. Trabalza, A., Eleftheriadou, I., Sgourou, A., Liao, T.-Y., Patsali, P., Lee, H., and Mazarakis, N. D. (2014) Enhanced central nervous system transduction with lentiviral vectors pseudotyped with RVG/HIV-1gp41 chimeric envelope glycoproteins. *J. Virol.* **88,** 2877–2890
61. Lei, Y., Joo, K. I., Wang, P. (2009) Engineering fusogenic molecules to achieve targeted transduction of enveloped lentiviral vectors. *J. Biol. Eng.* **3,** 8